ELSEVIER

Chemical Geology 200 (2003) 189–201

CHEMICAL GEOLOGY
INCLUDING
ISOTOPE GEOSCIENCE

www.elsevier.com/locate/chemgeo

Constraints on the origin of historic potassic basalts from northeast China by U–Th disequilibrium data

Haibo Zou[a,*], Mary R. Reid[a], Yongshun Liu[b], Yupeng Yao[c], Xisheng Xu[d], Qicheng Fan[e]

[a] *Department of Earth and Space Sciences, University of California at Los Angeles, Box 951567, 595 Charles E. Young Drive, Los Angeles, CA 90095-1567, USA*
[b] *Department of Geography, Beijing Normal University, Beijing 100037, China*
[c] *Institute of Geology and Geophysics, Chinese Academy of Sciences, Beijing 100029, China*
[d] *Department of Earth Sciences, Nanjing University, Nanjing 210093, China*
[e] *Institute of Geology, State Seismological Bureau, Beijing 100029, China*

Received 11 June 2002; accepted 6 May 2003

Abstract

The only historic eruptions of potassic basalts on the Earth reported so far took place in 1719–1721 AD in the Wudalianchi area of northeast China. These historic potassic basalts are characterized by significant ^{230}Th excesses [($^{230}Th/^{238}U$) = 1.24–1.33], and low $^{143}Nd/^{144}Nd$ ($\varepsilon_{Nd} = -5.0$ to -3.7) and $^{206}Pb/^{204}Pb$ (16.8–17.1). Strong ^{230}Th excesses, low $CaO + Al_2O_3$, and large bulk partition coefficients (D) in Rb, K, and Zr ($D_{Rb} \cong D_K > D_{Zr} > D_{Yb} > D_{Sm}$) inferred from a melt-normalized spider diagram suggest phlogopite-bearing garnet peridotites as dominant source rocks. The presence of garnet peridotites as mantle source, combined with negative ε_{Nd} in basalts and the geophysically determined lithosphere thickness in the study region (120 km), indicates the generation of these basalts at the depth of 80–120 km in the subcontinental lithospheric mantle. Dynamic melting inversion (DMI) of between-magma trace element concentration ratios and U–Th disequilibrium data suggests low-degree partial melting (5–7%) of a slow upwelling (< 1.6 cm/year) mantle source, although extremely low-degree batch partial melting (0.3–0.5%) of a static source is also possible. Source Nd model ages suggest that the source rocks for the Wudalianchi basalts were metasomatized at 1.0 Ga, provided that it has not experienced multistage enrichment history. Lithospheric extension since late Tertiary in the study region was responsible for slow decompression melting of phlogopite-bearing garnet peridotites in deep subcontinental lithospheric mantle. Recent (< 350 ka) subduction of the Pacific Plate may have produced lithospheric extension in the study region, but did not directly contribute subduction-related fluids to the source rocks for these potassic basalts because ^{230}Th enrichments are uncharacteristic of melts generated by subduction. The subducted slab may have lost fluids released from subducted sediments before the slab can reach the mantle beneath NE China.

Keywords: Historic basalts; Mantle melting; Mantle metasomatism; Basalt isotopes; Basalt trace elements; China basalts

* Corresponding author. Tel.: +1-310-794-5047; fax: +1-310-825-2779.
E-mail address: hzou@ess.ucla.edu (H. Zou).

0009-2541/03/$ - see front matter © 2003 Elsevier Science B.V. All rights reserved.
doi:10.1016/S0009-2541(03)00188-8

1. Introduction

Although potassic lavas are widely distributed on Earth (Bergman, 1987; Foley et al., 1987; Muller et al., 1992), historic eruptions of potassic basalts reported so far only occurred in the Wudalianchi (five big connected lakes) area, located at approximately 48°45′N, 126°10′E. The Quaternary (0.6 Ma–1721 AD) potassic volcanic fields, about 2000 km west of the active Pacific Plate margin, are situated on the northern margin of the Songliao Basin in NE China (Fig. 1), and consist of 14 individual volcanoes (Fig. 2) that cover an area of about 800 km^2. These potassic basalts represent an enriched mantle endmember for the diverse Cenozoic basalts in eastern China (Basu et al., 1991; Zhang et al., 1991; Zhou and Zhu, 1992; Zou et al., 2000) and are isotopically similar to EM1 (enriched mantle with low $^{143}Nd/^{144}Nd$ and moderate high $^{87}Sr/^{86}Sr$, as defined by Zindler and Hart, 1986). Two of the Wudalianchi cones, Laoheishan (old black hill) and Huoshaoshan (fire burning hill), erupted during 1719–1721 AD, according to the Qing Dynasty Records (Anonymous, 1720; Feng and Whitford-Stark, 1986; Wu, 1721). Thus, these historic lavas offer a unique opportunity to precisely quantify the magnitude of short-lived $^{238}U-^{230}Th$ disequilibrium (half-life of $^{230}Th = 75{,}000$ years, or 75 ka) at the time of eruption. We measured U–Th disequilibrium, together with Nd, Sr, and Pb isotopic compositions, in these historic lavas in order to gain insights into the origin of potassic magmas and the variability of subcontinental lithospheric mantle. Major and trace element analyses for the same basalts are also reported.

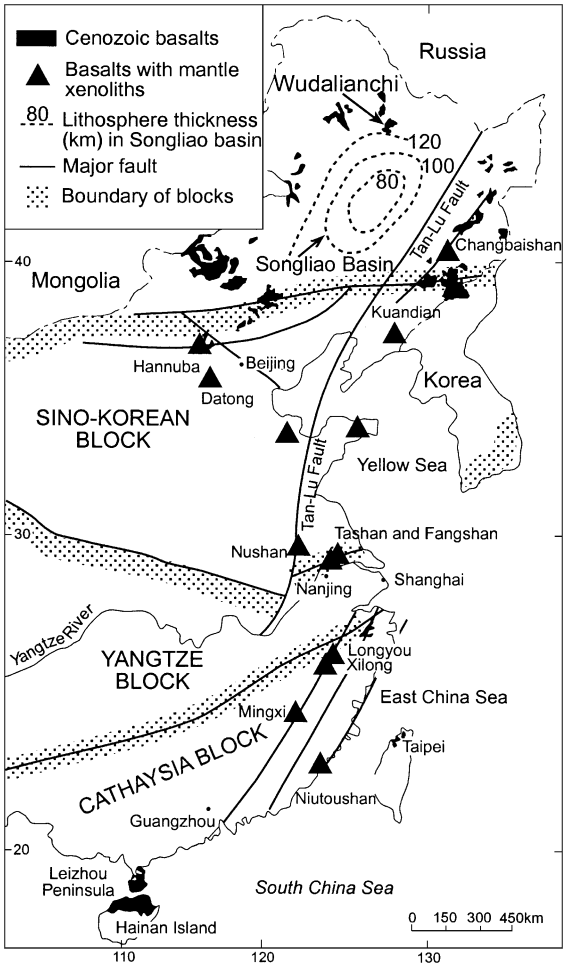

Fig. 1. Locations of the Wudalianchi basalts in NE China. The thickness of lithosphere in the Songliao Basin is from Ma (1987).

2. Methods

Th and Nd were measured using a VG 54-30 multicollector thermal ionization mass spectrometer equipped with a WARP filter and an ion counting system. Sr and Pb isotope ratios were measured by VG 54 Sector multicollector thermal ionization mass spectrometer at UCLA. Repeated analyses for Th isotopic standards are $^{232}Th/^{230}Th = 1.703 \times 10^5 \pm 1.5 \times 10^3$ ($n = 37$) [reported errors are 2× standard deviation (S.D.) throughout this paper] for UC Santa Cruz Th standard TML-1, which is in accord to the working value of $1.706 \times 10^5 \pm 1.4 \times 10^3$ (Collerson et al., 1997; Layne and Sims, 2000). Analyses of the Woods Hole–UCLA–National High Magnetic Field Laboratory standard (WUN-1) give $^{232}Th/^{230}Th = 2.303 \times 10^5 \pm 2.5 \times 10^3$ ($n = 6$), within error of the analyses obtained using ISOLAB 54 at the National High Magnetic Field Laboratory ($2.327 \times 10^5 \pm 2.4 \times 10^3$) (Zou et al., 2002), Cameca IMS 1270 at Woods Hole ($2.305 \times 10^5 \pm 2.3 \times 10^3$), and Finnigan Neptune at Woods Hole ($2.336 \times 10^5 \pm 1.5 \times 10^3$) (Ball et al., 2002). Reproducibility of $^{238}U/^{232}Th$ ratios is estimated to be <2%. Nd and Sr isotopic

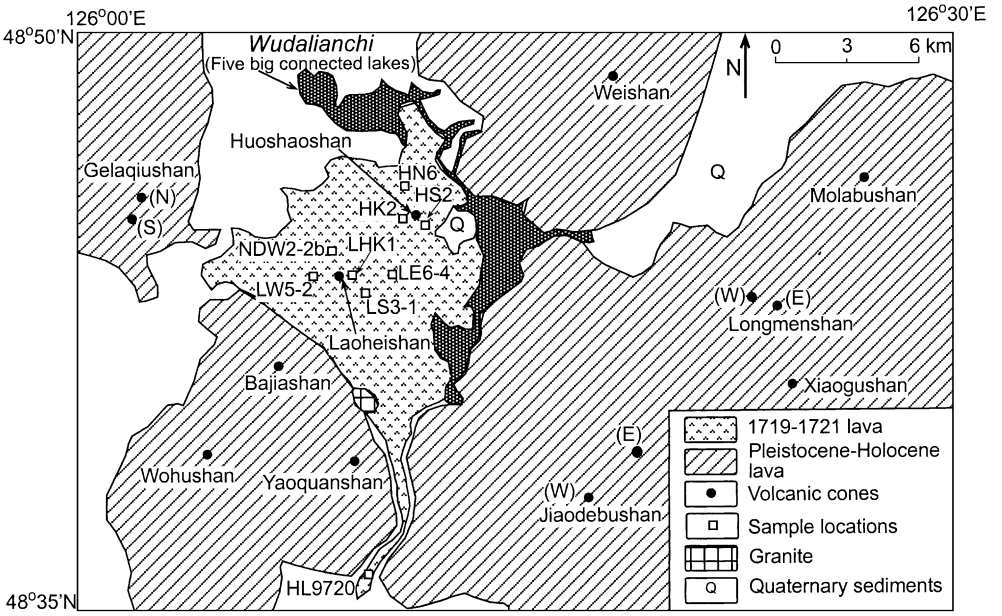

Fig. 2. A simplified geological map of the Wudalianchi volcanic field (Feng and Whitford-Stark, 1986) showing the locations of the 14 volcanoes and our sample locations in Huoshaoshan and Laoheishan.

compositions were normalized to $^{146}Nd/^{144}Nd = 0.7219$ and $^{86}Sr/^{88}Sr = 0.1194$, respectively. The measured Nd and Sr isotope standard values are $^{143}Nd/^{144}Nd = 0.511843 \pm 13$ ($n = 24$) for La Jolla and $^{87}Sr/^{86}Sr = 0.710239 \pm 16$ ($n = 13$) for NBS 987. Replicate analyses of Pb isotope standard NBS 981 give $^{206}Pb/^{204}Pb = 16.896 \pm 0.013$, $^{207}Pb/^{204}Pb = 15.435 \pm 0.014$, and $^{208}Pb/^{204}Pb = 36.525 \pm 0.041$. Relative to the following values for NBS981: $^{206}Pb/^{204}Pb = 16.9356$, $^{207}Pb/^{204}Pb = 15.4891$, and $^{208}Pb/^{204}Pb = 36.7006$ (Todt et al., 1996), Pb isotopic data in samples were corrected for mass fractionation of 0.12%/amu for $^{206}Pb/^{204}Pb$, $^{207}Pb/^{204}Pb$, and $^{208}Pb/^{204}Pb$. Major element abundances were obtained on fused La-bearing lithium borate glass disks using a Siemens MRS-400 multichannel, simultaneous X-ray spectrometer at the Ronald B. Gilmore XRF Laboratory of the University of Massachusetts at Amherst. Relative errors (2 S.D./mean) for major elements are: SiO_2 (0.4%), TiO_2 (0.4%), Al_2O_3 (0.4%), FeO (0.6%), MnO (1%), MgO (0.5%), CaO (0.2%), Na_2O (0.9%), K_2O (0.4%), and P_2O_5 (2%). Trace element concentrations of selected samples were measured by inductively coupled plasma (ICP) mass spectrometry by the GeoAnalytical Laboratory at the Washington State University. Relative errors for most trace element analyses are estimated to be <4%, except for Ta (6%), Cs (6%), Pb (7%), Sc (7%), Th (16%), and U (16%).

3. Results

Th, Sr, Nd, and Pb isotopic compositions as well as major element concentrations for the Wudalianchi basalts are presented in Table 1. Trace element concentrations on selected samples are given in Table 2. The samples have K_2O>4.4%, K_2O/Na_2O>1.1, and show significant enrichment in light rare earth elements (LREEs) (Fig. 3A). All basalts have high Th/U (4.5–5.0), similar to the results of the extremely potassic Gaussberg lamproites (Williams et al., 1992). On a primitive mantle-normalized spider diagram, the basalts display relative enrichment in Ba and K, and moderate depletion in Th, U, and Nb (Fig. 3B). Because the samples were ground in a tungsten carbide mill that may have increased Nb concentrations in powders, the basalts may have more negative Nb anomalies than the apparent ones.

Table 1
Major element concentrations (in wt.%) and isotopic compositions

Samples	LS3-1	LE6-4	LHK-1	LW5-2	HL9720	NDW2-2b	HK-2	HS2-2	HN6-1
Locations	Laohei	Laohei	Laohei	Laohei	Laohei	Laohei	Huoshao	Huoshao	Huoshao
SiO_2	53.48	50.97	51.42	51.08	53.36	53.52	50.37	48.90	51.13
TiO_2	2.43	2.28	2.30	2.53	2.32	2.33	2.22	2.34	2.25
Al_2O_3	13.88	13.32	13.31	13.20	14.17	13.86	13.37	13.00	13.53
Fe_2O_3[a]	8.15	8.94	8.85	9.04	7.45	8.01	9.21	9.64	9.00
MnO	0.12	0.13	0.13	0.13	0.13	0.12	0.14	0.15	0.13
MgO	5.92	7.68	7.65	6.86	5.87	6.01	7.67	7.88	7.25
CaO	5.49	6.67	6.50	6.57	5.11	5.40	7.58	8.03	7.12
Na_2O	3.68	3.90	3.85	3.83	3.81	4.00	3.94	4.12	3.82
K_2O	5.70	4.90	4.96	5.39	5.53	5.53	4.45	4.73	4.51
P_2O_5	1.06	1.00	0.99	1.15	0.98	1.03	1.02	1.18	0.93
Total	99.91	99.78	99.95	99.77	99.38	99.79	99.96	99.98	99.69
K_2O/Na_2O	1.55	1.26	1.29	1.41	1.45	1.39	1.13	1.15	1.18
Mg#[b]	0.63	0.66	0.67	0.64	0.64	0.63	0.66	0.65	0.65
$^{87}Sr/^{86}Sr$	0.705365	0.705189	0.705207	0.705295	0.705356	0.705350	0.705111	0.705054	0.705099
2 S.D.	0.000014	0.000011	0.000009	0.000011	0.000010	0.000010	0.000011	0.000013	0.000011
$^{143}Nd/^{144}Nd$	0.512380	0.512433	0.512425	0.512411	0.512383	0.512390	0.512443	0.512447	0.512439
2 S.D.	0.000008	0.000007	0.000009	0.000006	0.000011	0.000008	0.000007	0.000010	0.000008
ε_{Nd}[c]	−5.0	−4.0	−4.2	−4.4	−5.0	−4.8	−3.8	−3.7	−3.9
Sample $^{147}Sm/^{144}Nd$	0.1033	0.1067	NA	0.1032	NA	NA	NA	0.1048	0.1082
T_{sample} (Nd)[d]	943	900	NA	902	NA	NA	NA	868	904
Source $^{147}Sm/^{144}Nd$	0.1154	0.1154	0.1154	0.1154	0.1154	0.1154	0.1154	0.1154	0.1154
T_{source} (Nd)[e]	1050	973	985	1000	1040	1030	959	953	965
$^{208}Pb/^{204}Pb$	36.775	37.060	37.000	37.002	36.846	36.953	37.130	37.286	37.216
$^{207}Pb/^{204}Pb$	15.437	15.445	15.440	15.470	15.449	15.475	15.431	15.461	15.482
$^{206}Pb/^{204}Pb$	16.830	17.009	16.968	16.988	16.858	16.907	17.047	17.108	17.045
U (ppm)	1.32	1.48	1.43	1.52	1.50	1.49	1.39	1.63	1.31
Th (ppm)	6.08	6.77	6.66	6.77	6.66	6.86	6.76	8.18	6.08
Th/U	4.59	4.58	4.65	4.45	4.45	4.59	4.88	5.02	4.63
$(^{230}Th/^{232}Th)$	0.883	0.879	0.851	0.873	0.887	0.858	0.772	0.775	0.830
2 S.E.	0.009	0.008	0.010	0.007	0.010	0.007	0.006	0.006	0.008
$(^{238}U/^{232}Th)$	0.662	0.663	0.653	0.682	0.683	0.661	0.623	0.605	0.656
$(^{230}Th/^{238}U)$	1.334	1.326	1.302	1.280	1.298	1.297	1.239	1.282	1.265
2 S.E.	0.014	0.012	0.015	0.012	0.015	0.012	0.011	0.010	0.012

[a] Total iron as Fe_2O_3.

[b] $Mg\# = Mg^{2+}/(Mg^{2+} + Fe^{2+})$, assuming $Fe^{3+}/(Fe^{2+} + Fe^{3+}) = 0.15$.

[c] $\varepsilon_{Nd} = [(^{143}Nd/^{144}Nd)/(^{143}Nd/^{144}Nd)_{CHUR} - 1] \times 10^4$; $(^{143}Nd/^{144}Nd)_{CHUR} = 0.512638$.

[d] Sample Nd model age T is calculated using $^{143}Nd/^{144}Nd = 0.513114$ and $^{147}Sm/^{144}Nd = 0.222$ for depleted reservoir (DePaolo, 1988). Samples $^{147}Sm/^{144}Nd$ are obtained from Sm and Nd concentrations in Table 2. NA = not applicable due to lack of Sm and Nd concentrations.

[e] Source Nd model age is calculated using the same depleted reservoir but source Sm/Nd. Source $^{147}Sm/^{144}Nd$ is calculated using Sm = 0.73 ppm and Nd = 3.81 ppm (Table 3) from dynamic melting inversion, and is applied to both Laoheishan and Huoshaoshan. Source $^{143}Nd/^{144}Nd$ is the same as the sample $^{143}Nd/^{144}Nd$.

The basalts have negative ε_{Nd} (−5.0 to −3.7), high $^{87}Sr/^{86}Sr$ (0.70505–0.70536), and low $^{206}Pb/^{204}Pb$ (16.83–17.11). As with basalts from Northeastern China overall (Basu et al., 1991; Zou et al., 2000), Sr, Nd, and Pb isotope compositions in the Wudalianchi basalts display coherent variations and $^{87}Sr/^{86}Sr$ correlates negatively with $^{143}Nd/^{144}Nd$ and $^{206}Pb/^{204}Pb$ (Fig. 4A and B). Note that $^{206}Pb/^{204}Pb$ is negatively correlated with K_2O (Fig. 4C). The striking aspect of the Th isotope results is significant ^{230}Th excesses with $(^{230}Th/^{238}U) > 1.24$ (Fig. 5A). $(^{230}Th/^{232}Th)$ correlates positively with $^{87}Sr/^{86}Sr$ (Fig. 5B). As expected from Nd–Sr–Pb isotope correlations, $(^{230}Th/^{232}Th)$ correlates negatively with $^{143}Nd/^{144}Nd$ and $^{206}Pb/^{204}Pb$. Laoheishan basalts have higher $(^{230}Th/^{232}Th)$ and $^{87}Sr/^{86}Sr$, and lower $^{143}Nd/^{144}Nd$

Table 2
Trace element concentrations (ppm) and concentration ratios between HS2-2 and HN6-1

	LS3-1	LE6-4	LW5-2	HS2-2	HN6-1	(HS2-2)/(HN6-1)	Precision (2σ%)
La	94.1	85.8	96.4	111.9	80.1	1.397	4
Ce	169	151	171	195	142	1.373	2
Pr	18.9	16.9	19.1	21.8	16.1	1.354	2
Nd	68.4	62.1	69.7	80.0	59.4	1.347	3
Sm	11.8	11.0	12.0	13.9	10.7	1.299	4
Eu	3.15	2.94	3.23	3.75	2.93	1.280	4
Gd	8.29	7.94	8.62	9.81	7.84	1.251	2
Tb	1.00	0.97	1.04	1.19	0.97	1.227	2
Dy	4.74	4.70	4.90	5.64	4.64	1.216	3
Ho	0.77	0.76	0.80	0.90	0.75	1.200	3
Er	1.78	1.76	1.84	2.03	1.72	1.180	3
Tm	0.22	0.22	0.23	0.24	0.22	1.091	3
Yb	1.21	1.20	1.24	1.31	1.23	1.065	2
Lu	0.18	0.17	0.18	0.18	0.18	1.000	4
Ba	1684	1600	1834	1881	1558	1.207	4
Nb	66.6	66.6	70.4	70.6	57.9	1.219	4
Y	23.2	22.8	23.7	27.0	22.7	1.189	2
Hf	11.5	9.09	10.3	8.33	8.00	1.041	3
Ta	4.10	4.16	4.35	4.38	3.59	1.220	6
Pb	14.5	12.2	14.0	12.2	10.5	1.162	7
Rb	104.4	92.0	99.9	88.8	84.7	1.048	3
Cs	0.76	0.82	0.89	0.82	0.76	1.079	6
Sr	1494	1379	1479	1737	1350	1.287	3
Sc	10.8	13.4	13.0	12.1	13.1	0.924	7
Zr	502	396	444	363	344	1.055	3
Th	5.74	6.50	6.51	7.51	5.71	1.315	16
U	1.23	1.35	1.40	1.47	1.16	1.267	16

Relative two sigma precision values (2σ%) for trace element concentrations are reported in the last column. The U and Th concentrations from ICP-MS are consistent within 6–11% and 4–8%, respectively, with those from ID-TIMS (Table 1). These differences are well within the analytical errors for U and Th by ICP-MS.

and $^{206}Pb/^{204}Pb$, as compared with Huoshaoshan basalts.

4. Constraints on source rocks

4.1. Isotope constraints

The isotope correlations exhibited by the Wudalianchi basalts could reflect heterogeneities in the mantle source, or could be the result of assimilation of continental crust. Crustal materials (late Palaeozoic to Jurassic granites and pre-Permian schists) in the study region have higher $^{206}Pb/^{204}Pb$ (17.60–18.47) and $^{87}Sr/^{86}Sr$ (0.7052–0.7145) than these potassic basalts (Zhang et al., 1995). Contamination of the basalts by these upper crustal materials would be evident as a positive correlation in Sr–Pb isotope diagram, but the opposite is observed. In addition, the high incompatible element concentrations (e.g., Sr and Nd) in potassic magmas make their isotopic compositions less sensitive to crustal contaminations. Although the lower crust may have the required low $^{206}Pb/^{204}Pb$, significant ^{230}Th excesses indicate that these lavas ascended rapidly, which may have limited interactions with (upper and lower) crustal materials.

Strong ^{230}Th excesses in potassic basalts cannot be produced from crustal contaminations because bulk assimilation of crustal rocks with $(^{230}Th/^{238}U) = 1.0$ can only reduce the extent of ^{230}Th excesses. Deviations in $(^{230}Th/^{238}U)$ from unity could reflect the

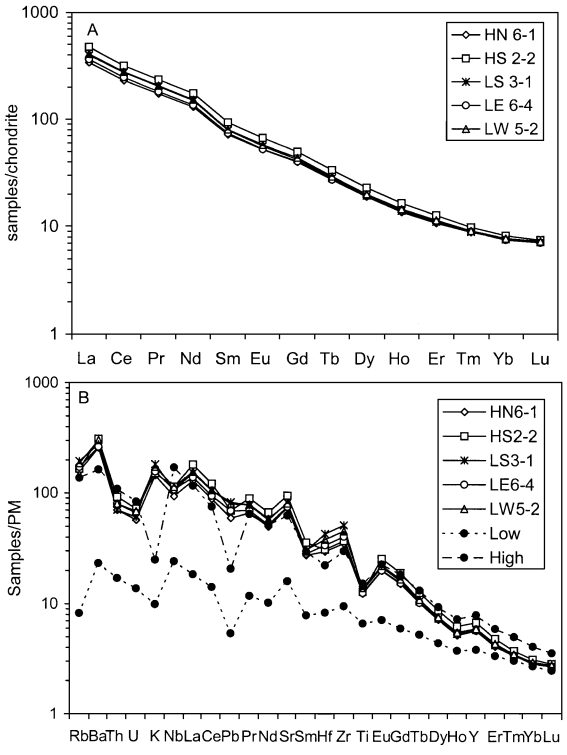

Fig. 3. (A) C1 chondrite-normalized REE abundance patterns for the historic potassic basalts. (B) Primitive mantle-normalized spider diagram for the Wudalianchi potassic basalts. Normalizing values are from Hofmann (1988). The area between the two dashed lines represents the range for basalts in other locations of eastern China.

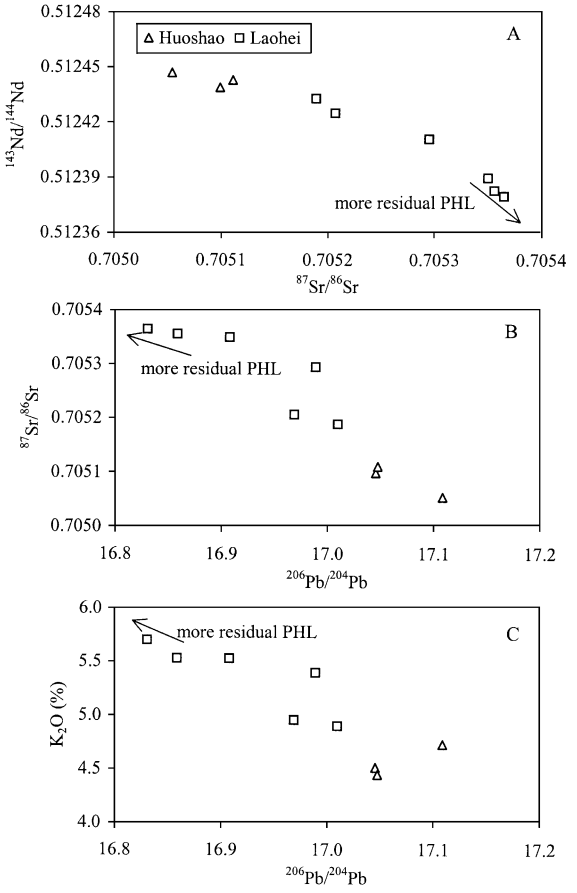

Fig. 4. Covariations in (A) $^{143}Nd/^{144}Nd$ vs. $^{87}Sr/^{86}Sr$, (B) $^{87}Sr/^{86}Sr$ vs. $^{206}Pb/^{204}Pb$, and (C) K_2O vs. $^{206}Pb/^{204}Pb$. PHL = phlogopite.

recent (< 350 ka, or five half-lives of ^{230}Th) metasomatic effects of fluids, or could be the result of partial melting. Because uranium is highly soluble and thorium is relatively insoluble in subduction-related fluids, addition of such fluids into the mantle often produces ^{238}U-enriched magmas (Elliott et al., 1997; Gill et al., 1991). Thus, although recent (< 350 ka) metasomatism by fluids derived from deeper mantle cannot be excluded, significant ^{230}Th excesses in all samples suggest that the potassic basalts are not directly related to the addition of fluids from sediments subducted beneath this portion of the circum-Pacific volcanic belt in the last 350 ka. Assuming, therefore, that the Th enrichment of the basalts is the result of the melting process, the extent of $^{238}U-^{230}Th$ disequilibrium depends on bulk partition coefficients of U and Th, melting rate, mantle porosity, and melting time (McKenzie, 1985; Williams and Gill, 1989; Zou and Zindler, 2000). Only the bulk partition coefficients of U and Th, and therefore the source mineralogy, determine whether ($^{230}Th/^{238}U$) is greater or less than 1. As garnet is the major mantle mineral that has $D_{Th}^{gt} \ll D_{U}^{gt}$ (Beattie, 1993; LaTourrette et al., 1993; Salters and Longhi, 1999), significant excesses in ^{230}Th [($^{230}Th/^{238}U$) = 1.24–1.33; Fig. 5A] in all samples indicate that the basaltic melts were produced in the presence of residual garnet. Although subcalcic clinopyroxenes under high pressure may have $D_{Th}^{cpx} < D_{U}^{cpx}$ (Landwehr et al., 2001; Turner et al., 1996; Wood et al., 1999) and may help explain ^{230}Th enrichment, Landwehr et al. (2001) have demonstrated that very small porosity (10^{-5}), small melting rate (10^{-5} kg/m^3/year), and high-pressure conditions (≥ 90 km) are all required to generate ($^{230}Th/^{238}U$) like those of the Wudalianchi basalts by melting of a spinel peridotite source. At such conditions, garnet would be normally stable and, given its D values for U and Th, would have the

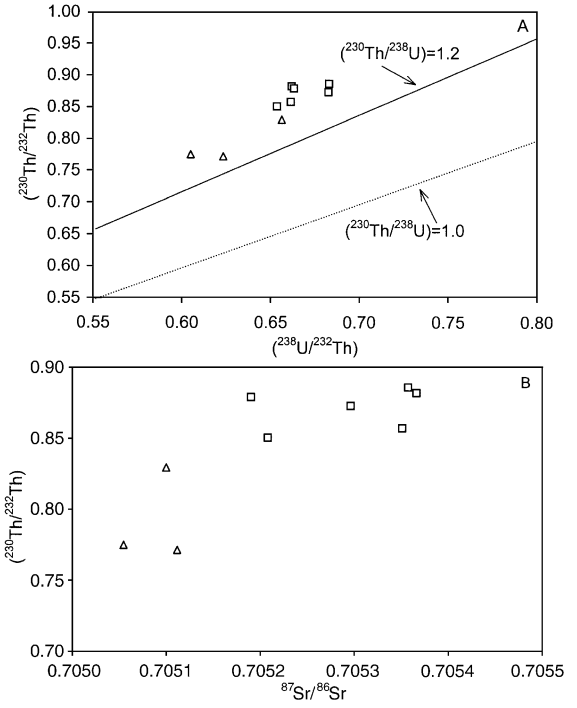

Fig. 5. Covariations in (A) ($^{230}Th/^{232}Th$) vs. ($^{238}U/^{232}Th$), and (B) ($^{230}Th/^{232}Th$) vs. $^{87}Sr/^{86}Sr$.

dominant role in ^{230}Th enrichment. Thus, we view the origin of the Wudalianchi basalts in the presence of residual garnet as necessary.

The strong correlation between ($^{230}Th/^{232}Th$) and ($^{238}U/^{232}Th$) (Fig. 5A) indicates that the range of ($^{230}Th/^{232}Th$) in the potassic basalts is mainly controlled by a range of ($^{238}U/^{232}Th$) ratio in the source. Because ($^{230}Th/^{232}Th$) also covaries with $^{87}Sr/^{86}Sr$ (Fig. 5B), $^{143}Nd/^{144}Nd$, and $^{206}Pb/^{204}Pb$, the correlation between ($^{230}Th/^{232}Th$) and ($^{238}U/^{232}Th$) is more likely due to source heterogeneity rather than an isochron. Similarly, the systematic correlations among $^{87}Sr/^{86}Sr$, $^{143}Nd/^{144}Nd$, $^{206}Pb/^{204}Pb$, and K_2O (Fig. 4) can be attributed to variable contributions from two components in a mixed mantle source—one that apparently has variable proportions of garnet peridotite and a metasomatic component. In this case, we prefer a petrogenetic model of melting of a mantle with small-scale heterogeneity (composite source model) in our case rather than mixing of melts from two large-scale mantle source regions. High K_2O contents (>4.4 wt.%) in the Wudalianchi basalts may require the presence of a potassic phase, most likely phlogopite, in the mantle source of these basalts. Since phlogopites often have high Rb/Sr and Pb/U (Ionov and Hofmann, 1995; Rosenbaum, 1993), high $^{87}Sr/^{86}Sr$ and low $^{206}Pb/^{204}Pb$ in Wudalianchi basalts are also consistent with the presence of phlogopite. Melting a mantle source with more phlogopite-bearing metasomatic component can produce melt with higher K_2O and $^{87}Sr/^{86}Sr$ but lower $^{206}Pb/^{204}Pb$.

4.2. Trace element constraints

The trace element data support the interpretation from isotopic data that both residual garnet and phlogopite are present in the source. Here we use ‘‘between-magma concentration ratios’’ (Zou and Zindler, 1996) or ‘‘enrichment ratios’’ (Class and Goldstein, 1997) to constrain relative elemental compatibility and thus source mineralogy. The method is essentially to normalize trace element concentrations in primary basalts by another cogenetic basalt, and we call it a melt-normalized spider diagram. This melt-normalized spider diagram is conceptually equivalent to the ‘‘enrichment ratio pattern’’ proposed by Class and Goldstein (1997) to evaluate the source mineralogy of Grande Comore, although Class and Goldstein (1997) obtained enrichment ratios from element variation diagrams. The requirements to build such a melt-normalized spider diagram are the same as those for dynamic melting inversion (DMI) (Zou and Zindler, 1996; Zou et al., 2000): (1) selected lavas have the same isotopic compositions and have high Mg# to avoid significant fractional crystallization; (2) highly incompatible and less-so-highly incompatible elements have large but different between-magma concentration ratios formed at different degrees of partial melting; and (3) low-degree (f_1) melt/high-degree (f_2) melt concentration ratios (Q) for rare earth elements satisfy a regular order according to their bulk distribution coefficients ($Q_{La}>Q_{Ce}>Q_{Nd}>Q_{Sm}>Q_{Lu}$). Such melt-normalized Q value is inversely correlated with D, and is independent of source concentrations.

Laoheishan basalts are similar in their trace element concentrations (Table 2) and consequently do not

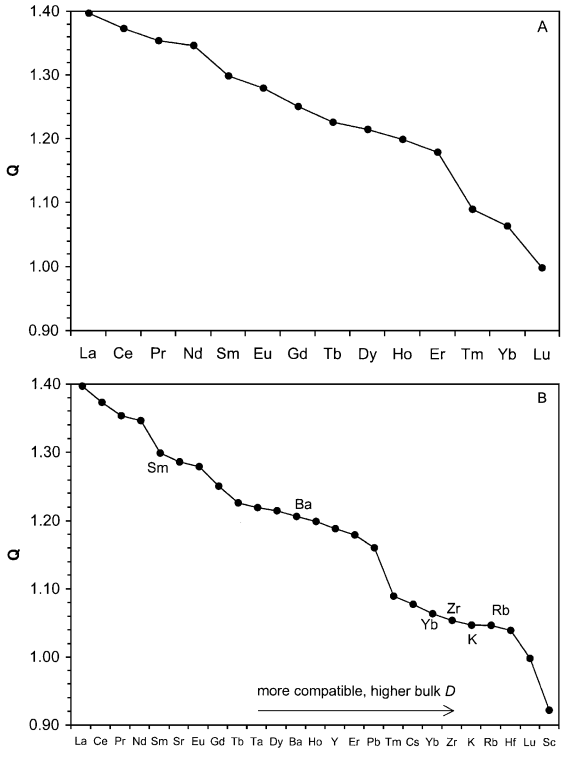

Fig. 6. (A) Rare earth element concentration ratios (HS2-2/HN6-1) decrease from Q_{La} to Q_{Lu}, satisfying requirement 3 for partial melting inversion. (B) A melt-normalized spider diagram for Huoshaoshan basalts using between-magma concentration ratios to identify elemental compatibility for the Wudalianchi mantle source.

reflect significantly different degrees of partial melting (requirement 2). In contrast, the two Huoshaoshan basalts (HN6-1 and HS2-2) have large but different concentration ratios (Fig. 6A) and generally satisfy all requirements (Tables 1 and 2). Dividing trace element concentrations in HS2-2 by HN6-1, and then sorting these between-magma concentration ratios, we obtain such a melt-normalized spider diagram for Huoshaoshan (Fig. 6B). Since lower Q values indicate higher D (more compatible), Fig. 6B demonstrates that Zr is more compatible than Sm and even Yb ($D_{Zr}>D_{Yb}>D_{Sm}$). This is consistent with the presence of residual garnet in the source rocks because $D_{Zr}>D_{Sm}$ in garnet peridotite whereas the opposite is true for spinel peridotite (McDade et al., in press). Similarly, K and Rb are more compatible than Sm and even Yb ($D_{Rb}\cong D_K>D_{Yb}>D_{Sm}$), strongly suggesting the presence of residual phlogopite that preferentially retains K and Rb in the source rocks.

4.3. Major elements and geophysical constraints

Garnet- and phlogopite-bearing source rocks could be garnet pyroxenites or garnet peridotites. If garnet pyroxenites are the source rocks, the partial melts would be enriched in Al_2O_3 and especially CaO (Hirschmann and Stolper, 1996; Kogiso and Hirschmann, 2001). However, $CaO+Al_2O_3$ in these potassic basalts are even lower than other Cenozoic alkali basalts in northeast China (Fig. 7). Therefore, we suggest that the dominant source rocks are garnet peridotites rather than garnet pyroxenites. For garnet peridotites to be present in the source, the initiation of melting must have occurred at depths >80 km. To estimate the maximum depth of melting, we use Nd isotopic compositions and geophysical evidence. Because asthenospheric mantle source produces basalts with positive ε_{Nd}, the negative ε_{Nd} values (-5.0 to -3.7) suggest that the mantle source is most likely to be lithospheric mantle. Since the thickness of lithosphere in the study region determined geophysically is about 120 km (Fig. 1) (Ma, 1987; Xu, 1996), we regard 120 km as the maximum depth. Therefore, the potassic basalts are likely derived from depths of 80–120 km.

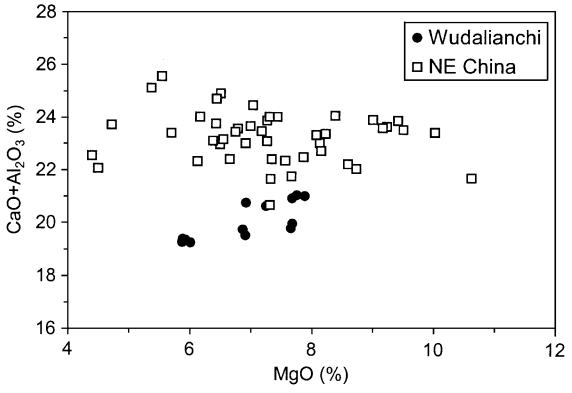

Fig. 7. $CaO+Al_2O_3$ vs. MgO plot. Data sources: Zhi et al. (1990), Basu et al. (1991), Zhang et al. (1991), Liu et al. (1994), and Zou (unpublished data).

5. Quantitative modeling

The magnitude of ($^{230}Th/^{238}U$) ratios in basalts can be used to constrain the conditions of melting (Beattie, 1993; Sims et al., 1999). If the source rocks are static in a closed system before instantaneous melt extraction begins, then net elemental fractionation is the cause of the U–Th disequilibrium and, based on the batch melting equation of Shaw (1970), we have:

$$\left(^{230}Th/^{238}U\right) = \left(^{230}Th/^{238}U\right)_0 \frac{D_U + f(1-D_U)}{D_{Th} + f(1-D_{Th})}. \quad (1)$$

Rearranging Eq. (1), we obtain:

$$f = \left(D_U - D_{Th}\frac{\left(^{230}Th/^{238}U\right)}{\left(^{230}Th/^{238}U\right)_0}\right) \Big/ \left((1-D_{Th})\frac{\left(^{230}Th/^{238}U\right)}{\left(^{230}Th/^{238}U\right)_0} - (1-D_U)\right) \quad (2)$$

where D_U and D_{Th} are bulk partition coefficients for U and Th, respectively, and f is the total degree of partial melting. For a secular equilibrium source, or $\left(^{230}Th/^{238}U\right)_0 = 1.0$, to produce $\left(^{230}Th/^{238}U\right) = 1.24$–$1.33$ in melts, the calculated partial melting degrees from Eq. (2) vary from 0.53% to 0.31% (Fig. 8).

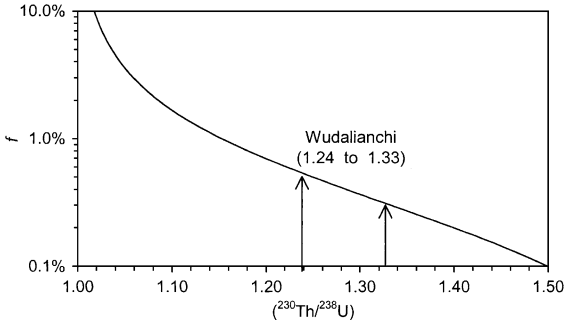

Fig. 8. Estimates of the degrees of partial melting from (^{230}Th/^{238}U) using Eq. (2). Bulk partition coefficients are $D_U = 0.005$ and $D_{Th} = 0.003$ for garnet peridotites. Bulk partition coefficients are given by $D_i = \Sigma K_i x_i$, where K_i is the mineral/melt partition coefficient and x_i is its mineral proportion in the source. Mineral/melt partition coefficients are: K_{Th} (gt) = 0.019, K_U (gt) = 0.041, K_{Th} (opx) = 0.0002, K_U (opx) = 0.0005 (Salters and Longhi, 1999), K_{Th} (cpx) = 0.015, K_U (cpx) = 0.010 (Lundstrom et al., 1994), K_{Th} (phl) = 0.0011, K_U (phl) = 0.0014 (LaTourrette et al., 1995), K_{Th} (ol) = K_U (ol) = 0.0001 (assumed). Mineral proportions are: $x_{ol} = 57\%$, $x_{opx} = 17\%$, $x_{gt} = 10\%$, $x_{cpx} = 6\%$, and $x_{phl} = 10\%$. Mineral abbreviations: gt = garnet, opx = orthopyroxene, cpx = clinopyroxene, ol = olivine, and phl = phlogopites.

The requirement of very low degrees of melting (< 0.5%) can be relaxed somewhat if the solid mantle has been upwelling. Indeed, the study region has been undergoing extension since late Tertiary (Ma, 1987). The extension is manifested by formation and remobilization of a graben and several high-angle normal faults around the Wudalianchi fields (Zhang et al., 1991). Both the inversion of geopotential data (Liu, 1978) and earthquake focal mechanism solutions (Ma, 1987) suggest that, at present, the Wudalianchi area and adjacent regions are still under a tensile stress field. For a dynamic upwelling mantle source, we need to consider the ingrowth of ^{230}Th within the residual solid in the melting column (e.g., Elliott, 1997). There are two ingrowth models: dynamic melting model (McKenzie, 1985; Williams and Gill, 1989; Zou and Zindler, 2000) and equilibrium percolation model (Spiegelman and Elliott, 1993). Dynamic melting is a "zero-Damkohler number" model (melt–solid reaction is very slow relative to melt migration velocity) whereas the latter is an "infinite Damkohler number" model (melt–solid reaction is very fast relative to melt migration velocity) (Sims et al., 1999). In all likelihood, reality lies somewhere between the two endmember models (Hart, 1993). Since the equilibrium percolation model involves varying parameters, it is unlikely to invert these parameters from one measurement in (^{230}Th/^{238}U). We thus choose dynamic melting model for inversion by rewriting Eq. (30) in Zou and Zindler (2000) as:

$$\dot{M} = \frac{(\lambda_{238} + \lambda_{230})[\rho_f \phi + \rho_s (1-\phi) D_U] - Z\lambda_{230}[\rho_f \phi + \rho_s (1-\phi) D_{Th}]}{(Z-1)[1 + \rho_f \phi / [\rho_s (1-\phi)]]} \quad (3)$$

where Z represents measured (^{230}Th/^{238}U) activity ratios, ϕ is the melting porosity, $\dot{M}$ is the melting rate, and ρ_f and ρ_s represent the density of melt and solid, respectively. It should be emphasized that in the dynamic melting model, there is replenishment of materials to the melting column from below, and the melting rate is closely related to mantle upwelling rate and melt productivity. Because we have only one equation but two unknowns in $\dot{M}$ and ϕ, we cannot obtain unique solutions for $\dot{M}$ and ϕ but can, nevertheless, put some quantitative constraints on these variables. Melting rates and porosity in a garnet peridotite source that satisfy this relationship for a given value of (^{230}Th/^{238}U) are shown in Fig. 9. For melting rates to be non-negative, the melting porosity ϕ must be < 0.6%. For non-negative values of ϕ, the melting rate $\dot{M}$ must be $< 1.6 \times 10^{-4}$ (kg/m^3/year) (Fig. 9). The melting rate can be used to estimate solid mantle upwelling velocity (W) in a one-dimensional

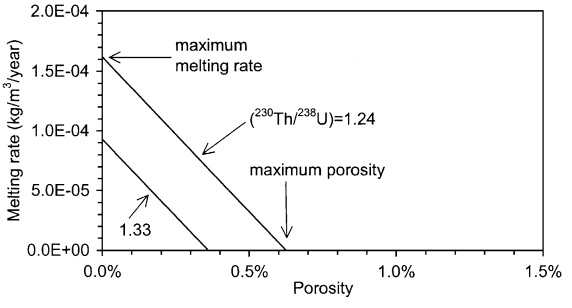

Fig. 9. Constraints on melting rate and porosity from (^{230}Th/^{238}U) using Eq. (3). $\rho_f = 2800$ kg/m^3 and $\rho_s = 3300$ kg/m^3. Bulk partition coefficients are the same as in Fig. 8. Because both K_{Th} (phl) and K_U (phl) are small and similar, the presence of phlogopites in the garnet peridotite source does not significantly affect U–Th disequilibrium. Note that if ϕ is very small, we have $[1 + \rho_f \phi / [\rho_s (1-\phi)]] \approx 1$, then $\dot{M}$ has a near-linear relationship with ϕ in Eq. (3), resulting in near-straight lines in figure.

melting column, by rewriting Eq. (7) in Sims et al. (1999) as:

$$W = \frac{\dot{M}}{\rho_s(\mathrm{d}f/\mathrm{d}z)} \quad (4)$$

where z (in km) represents the depth at a melting column. If the melt productivity $\mathrm{d}f/\mathrm{d}z = 0.003\ \mathrm{km}^{-1}$ is used (Asimow et al., 1997; McKenzie and Bickle, 1988), then the maximum solid mantle upwelling rate W is about 1.6 cm/year. The inference of slow upwelling is consistent with the fact that the Wudalaichi basalts are situated on the margin (rather than the center) of the Songliao Basin.

The degree of partial melting (f) for dynamic melting cannot be obtained from the U–Th disequilibrium data because f is determined by melting rate, porosity, and melting time (Eq. (40) in Zou and Zindler, 2000) and, as illustrated above, is not unique. However, we can apply the dynamic melting inversion method to obtain f from between-magma trace element concentrations ratios (Zou and Zindler, 1996; Zou et al., 2000). The DMI method uses variations of between-magma concentration ratios (Q) for two incompatible elements that have different bulk partition coefficients, and does not require assumptions regarding source-incompatible element concentrations or ratios. The advantage for this approach is that the degree of partial melting and source compositions can be calculated independently. It has been demonstrated that DMI is an effective method for studying the petrogenesis of basalts (e.g., Lustrino et al., 2002; Zhang et al., 2002).

For dynamic partial melting inversion, the highly incompatible element has a bulk partition coefficient D_a of about 0.001, and the ideal D_b for the less-so-highly incompatible element would be between 0.01 and 0.1, so that Q_b is different enough from Q_a and from 1.0. Thus, La is suitable for D_a, and Nd, Sm, Eu, Gd, and Tb are suitable for D_b. As mentioned above, the pair of HN6-1 and HS2-2 from Huoshaoshan satisfies the DMI requirements. The La concentration ratio (HS2-2/HN6-1) is taken as Q_a, and the Sm concentration ratio is used to derive Q_b for this pair:

$$Q_a = Q_{La} = 111.9/80.1 = 1.397$$

$$Q_b = Q_{Sm} = 13.9/10.7 = 1.299.$$

Because our U–Th disequilibrium data require that ϕ must be $<0.6\%$, we choose $\phi = 0.4\%$ for the Wudalianchi basalts. Using these concentration ratios and ϕ, and solving the system of Eqs. (3) and (4) in Zou et al. (2000), we obtain $X_1 = 4.54\%$ and $X_2 = 6.34\%$. Substituting these values into Eq. (5) in Zou et al. (2000), we have $f_1 = 4.86\%$ for HS2-2 and $f_2 = 6.65\%$ for HN6-1. Similarly, using the La concentration ratio for Q_a, but Nd, Eu, Gd, or Tb (instead of Sm) to obtain Q_b, four additional sets of f_1 and f_2 can be obtained. Averaging all the obtained values yields $X_1 = 4.62\%$, $f_1 = 5.00\%$, $X_2 = 6.48\%$, and $f_2 = 6.85\%$. Substituting these average values for X_1 or X_2 into Eq. (1) in Zou et al. (2000), we can calculate source concentrations (C_0) for La, Nd, Sm, Eu, Gd, and Tb, respectively (Table 3). The DMI results clearly demonstrate a small degree (4–7%) of partial melting of an LREE-enriched source.

Source Sm and Nd concentrations calculated from DMI can be used to better constrain the source Nd model ages for Huoshaoshan. Sample Nd model ages are calculated as about 900 Ma (Table 1); however, sample Nd model ages are minimum ages because Sm/Nd ratios in melts are smaller than source Sm/Nd ratios. According to DMI results, source Sm/Nd = 0.73/3.81 = 0.1916, which is about 10% higher than sample Sm/Nd. If we use source Sm/Nd ratio of 0.1916 for Huoshaoshan and assume a similar source Sm/Nd for Laoheishan, then the calculated source Nd model ages are about 1000 Ma (Table 1). If there is no multistage history of mantle enrichments in the

Table 3
Calculation of partial melting degrees and mantle source compositions for the Huoshaoshan basalts

	D	HS2-2	HN6-1	Q	f_1 (%)	f_2 (%)	C_0	$(C_0)_N$
La	0.0021	111.9	80.1	1.397			5.17	21.9
Nd	0.0095	80.0	59.4	1.347	4.07	5.56	3.81	8.3
Sm	0.0180	13.9	10.7	1.299	4.86	6.65	0.73	4.9
Eu	0.0228	3.75	2.93	1.280	5.29	7.26	0.21	3.7
Gd	0.0279	9.81	7.84	1.251	5.35	7.35	0.59	3.0
Tb	0.0330	1.19	0.97	1.227	5.42	7.44	0.076	2.1
Average					5.00	6.85		

The bulk partition coefficients are the same as Zou and Zindler (1996) for garnet peridotites. $\Phi = 0.4\%$. Increasing Φ from 0.4% to 0.5% results in an increase in f by about 0.2%, and decreasing Φ from 0.4% to 0.3% results in a decrease in f by about 0.2%. REE abundances for C1 chondrites to normalize source concentration C_0 are from Anders and Ebihara (1982).

source, then 1000 Ma may be regarded as the age for this enrichment source. The coherent variations in Sr, Nd, and Pb isotopic ratios (Fig. 4) suggest that the mantle metasomatism could be either a single event or an episodic or continuous process by melts with similar geochemical signatures (Bailey, 1982). U–Th disequilibrium data argue against recent (<350 ka) source enrichment by subduction-related fluids, but cannot preclude other possible enrichment events between 1000 Ma and 350 ka.

6. Concluding remarks

The Wudalianchi potassic basalts of northeastern China are characterized by strong excess of ^{230}Th relative to ^{238}U, by unradiogenic Pb and Nd and radiogenic Sr isotope ratios, and by large enrichments in incompatible trace elements. Phlogopite-bearing garnet peridotites as source rocks are suggested from significant enrichment in ^{230}Th relative to ^{238}U, and low $CaO + Al_2O_3$. Large partition coefficients in K, Rb, and Zr ($D_{Rb} \cong D_K > D_{Zr} > D_{Yb} > D_{Sm}$) inferred from the melt-normalized spider diagram also support the presence of residual garnet and phlogopite in the source. The depth of partial melting is estimated as 80–120 km based on the presence of residual garnet, the negative ε_{Nd} (indicative of subcontinental lithospheric mantle origin), and the thickness of the lithosphere in the study region (120 km). Dynamic melting inversion of trace element concentration ratios and U–Th disequilibrium data suggest low-degree partial melting (5–7%) of a slow upwelling (<1.6 cm/year) mantle source, although U–Th disequilibrium data can also be explained by an extremely low degree of batch partial melting (0.3–0.5%) of a static source. We prefer the dynamic melting model because the mantle in the study region has been upwelling since late Tertiary. Since ^{230}Th enrichments are uncharacteristic of melts generated by subduction, the source rocks were not metasomatized by fluids released during subduction of the Pacific sediments in the last 350 ka. The significant ^{230}Th excesses in the potassic basalts contrast with the near-secular equilibrium in many low ε_{Nd} basalts derived from subcontinental lithospheric mantle in southwest United States (Asmerom, 1999; Asmerom and Edwards, 1995; Reid, 1995; Reid and Ramos, 1996), indicating the different melting parameters and variability in the compositions of the subcontinental lithospheric mantle. Further studies are needed in order to identify/isolate the dominating factor(s) in making these differences in U–Th disequilibrium in subcontinental mantle-derived basalts.

Acknowledgements

We are grateful to Simon Turner, Yemane Asmerom, and Editor Steve Goldstein for their constructive reviews that significantly improved the quality of this paper. We are also indebted to An Yin, James Gill, Ken Sims, and Jorge Vazquez for fruitful discussion and help. This work was supported by the National Science Foundation [EAR 9805687 (an NSF postdoctoral research fellowship) to Zou and EAR 9980646 to Reid], by the Natural Science Foundation of China (49802006 to Liu), and by the Geological Society of America (6744-00 to Zou). **[SG]**

References

Anders, E., Ebihara, M., 1982. Solar-system abundances of the elements. Geochim. Cosmochim. Acta 46, 2363–2380.

Anonymous, 1720. Notes on Heilongjiang. The Qing Dynasty Records.

Asimow, P.D., Hirschmann, M.M., Stolper, E.M., 1997. An analysis of variations in isentropic melt productivity. Philos. Trans. R. Soc. Lond., A 355, 255–281.

Asmerom, Y., 1999. Th–U fractionation and mantle structure. Earth Planet. Sci. Lett. 166, 163–175.

Asmerom, Y., Edwards, R.L., 1995. U-series isotope evidence for the origin of continental basalts. Earth Planet. Sci. Lett. 134, 1–7.

Bailey, D.K., 1982. Mantle metasomatism—continuing chemical change within the Earth. Nature 296, 525–530.

Ball, L., Sims, K.W.W., Weyer, S., Schwieters, J., 2002. Measurement of $^{232}Th/^{230}Th$ in volcanic rocks by PIMMS, using the ThermoFinnigan Neptune. Geochim. Cosmochim. Acta 66, A47.

Basu, A.R., Wang, J.W., Huang, W.K., Xie, G.H., Tatsumoto, M., 1991. Major element, REE, and Pb, Nd and Sr isotopic geochemistry of Cenozoic volcanic rocks of eastern China: implications for their origin from suboceanic-type mantle reservoirs. Earth Planet. Sci. Lett. 105, 149–169.

Beattie, P., 1993. Uranium–thorium disequilibria and partitioning on melting of garnet peridotite. Nature 363, 63–65.

Bergman, S.C., 1987. Lamproites and other potassium-rich igneous rocks: a review of their occurrence, mineralogy and geochemistry. In: Fitton, J.G., Upton, B.G.J. (Eds.), Alkaline Igneous

Rocks. Geological Society Special Publication. Blackwell Scientific Publications, Oxford, pp. 103–190.
Class, C., Goldstein, S.L., 1997. Plume–lithosphere interactions in the ocean basins: constraints from the source mineralogy. Earth Planet. Sci. Lett. 150, 245–260.
Collerson, K.D., Palacz, Z., Turner, P.J., 1997. Precise measurement of U-series nuclides by high sensitivity magnetic sector multicollector ICP-MS. EOS 78, F788.
DePaolo, D.J., 1988. Neodymium Isotope Geochemistry: An Introduction. Springer, Berlin. 187 pp.
Elliott, T., 1997. Fractionation of U and Th during mantle melting: a reprise. Chem. Geol. 139, 165–183.
Elliott, T., Plank, T., Zindler, A., White, W., Bourdon, B., 1997. Elemental transport from slab to volcanic front at the Mariana arc. J. Geophys. Res. 102, 14991–15019.
Feng, M.S., Whitford-Stark, J.L., 1986. The 1719–1721 eruptions of potassium-rich lavas at Wudalianchi, China. J. Volcanol. Geotherm. Res. 30, 131–148.
Foley, S.F., Venturelli, G., Green, D.H., Toscani, L., 1987. The ultrapotassic rocks: characteristics, classification, and constraints for petrogenetic models. Earth Sci. Rev. 24, 81–134.
Gill, J.B., Pyle, D.M., Williams, R.W., 1991. Igneous rocks. In: Heaman, L., Ludden, J.N. (Eds.), Applications of Radiogenic Isotope Systems to Problems in Geology. Mineralogical Association of Canada, Toronto, pp. 287–335.
Hart, S.R., 1993. Equilibration during mantle melting: a fractal tree model. Proc. Natl. Acad. Sci. 90, 11914–11918.
Hirschmann, M.M., Stolper, E.M., 1996. A possible role for garnet pyroxenite in the origin of the "garnet signature" in MORB. Contrib. Mineral. Petrol. 124, 185–208.
Hofmann, A.W., 1988. Chemical differentiation of the Earth: the relationship between mantle, continental crust, and the oceanic crust. Earth Planet. Sci. Lett. 90, 297–314.
Ionov, D.A., Hofmann, A.W., 1995. Nb–Ta-rich mantle amphiboles and micas: implications for subduction-related metasomatic trace element fractionations. Earth Planet. Sci. Lett. 131, 341–356.
Kogiso, T., Hirschmann, M.M., 2001. Experimental study of clinopyroxene partial melting and the origin of ultra-calcic melt inclusions. Contrib. Mineral. Petrol. 142, 347–360.
Landwehr, D., Blundy, J., Chamorro-Perez, E.M., Hill, E., Wood, B., 2001. U-series disequilibrium generated by partial melting of spinel lherzolite. Earth Planet. Sci. Lett. 188, 329–348.
LaTourrette, T.Z., Kennedy, A.K., Wasserburg, G.J., 1993. Thorium–uranium fractionation by garnet: evidence for a deep source and rapid rise of oceanic basalts. Science 261, 739–742.
LaTourrette, T., Hervig, R.L., Holloway, J.R., 1995. Trace element partitioning between amphibole, phlogopite, and basanite melt. Earth Planet. Sci. Lett. 135, 13–30.
Layne, G.D., Sims, K.W.W., 2000. Secondary ion mass spectrometry for the measurement of $^{232}Th/^{230}Th$ in volcanic rocks. Int. J. Mass Spectrom. 203, 187–198.
Liu, H.S., 1978. Mantle convection pattern and subcrustal stress field under Asia. Phys. Earth Planet. Inter. 16, 247–256.
Liu, C.Q., Masuda, A., Xie, G.H., 1994. Major- and trace-element compositions of Cenozoic basalts in east China: petrogenesis and mantle source. Chem. Geol. 114, 19–42.
Lundstrom, C.C., Shaw, H.F., Ryerson, F.J., Phinney, D.L., Gill, J.B., Williams, Q., 1994. Compositional controls on the partitioning of U, Th, Ba, Pb, Sr, and Zr between clinopyroxene and haplobasaltic melts: implications for uranium series disequilibria in basalts. Earth Planet. Sci. Lett. 128, 407–423.
Lustrino, M., Melluso, L., Morra, V., 2002. The transition from alkaline to tholeiitic magmas: a case study from the Orosei–Dorgali Pliocene volcanic district (NE Sardinia, Italy). Lithos 63, 83–113.
Ma, X.Y., 1987. Lithospheric Dynamics Map of China and Adjacent Seas (1:4,000,000) and Explanatory Notes. Geological Publishing House, Beijing. 53 pp.
McDade, P., Blundy, J., Wood, B., in press. Trace element partitioning on the Tinaquillo lherzolite solidus at 1.5 GPa. Phys. Earth Planet. Inter.
McKenzie, D., 1985. $^{230}Th-^{238}U$ disequilibrium and the melting processes beneath ridge axes. Earth Planet. Sci. Lett. 72, 149–157.
McKenzie, D., Bickle, M.J., 1988. The volume and composition of melt generated by extension of the lithosphere. J. Petrol. 29, 625–679.
Muller, D., Rock, N.M.S., Groves, D.I., 1992. Geochemical discrimination between shoshonitic and potassic volcanic rocks in different tectonic settings: a pilot study. Mineral. Petrol. 46, 259–289.
Reid, M.R., 1995. Processes of mantle enrichment and magmatic differentiation in the eastern Snake River Plain: Th isotope evidence. Earth Planet. Sci. Lett. 131, 239–254.
Reid, M.R., Ramos, F.C., 1996. Chemical dynamics of enriched mantle in the southwestern United States: thorium isotope evidence. Earth Planet. Sci. Lett. 138, 67–81.
Rosenbaum, J.M., 1993. Mantle phlogopite: a significant lead repository? Chem. Geol. 106, 475–483.
Salters, V.J.M., Longhi, J., 1999. Trace element partitioning during the initial stages of melting beneath mid-ocean ridges. Earth Planet. Sci. Lett. 166, 15–30.
Shaw, D.M., 1970. Trace element fractionation during anatexis. Geochim. Cosmochim. Acta 34, 237–243.
Sims, K.W.W., DePaolo, D.J., Murrell, M.T., Baldredge, W.S., Goldstein, S., Clague, D., Jull, M., 1999. Porosity of the melting zone and variations in the solid mantle upwelling rate beneath Hawaii: inferences from $^{238}U-^{230}Th-^{226}Ra$ and $^{235}U-^{231}Pa$ disequilibria. Geochim. Cosmochim. Acta 63, 4119–4138.
Spiegelman, M., Elliott, T., 1993. Consequences of melt transport for uranium series disequilibrium in young lavas. Earth Planet. Sci. Lett. 118, 1–20.
Todt, W., Cliff, R.A., Hanser, A., Hofmann, A.W., 1996. Evaluation of a $^{202}Pb-^{205}Pb$ double spike for high-precision lead isotope analysis. In: Basu, A.R., Hart, S.R. (Eds.), Earth Processes: Reading the Isotopic Code. Geophysical Monograph. American Geophysical Union, Washington, DC, pp. 429–437.
Turner, S., et al., 1996. Post-collision, shoshonitic volcanism on the Tibetan Plateau: implications for convective thinning of the Lithosphere and the Source of ocean island basalts. J. Petrol. 37 (1), 45–71.
Williams, R.W., Gill, J.B., 1989. Effect of partial melting on the uranium decay series. Geochim. Cosmochim. Acta 53, 1607–1619.

Williams, R.W., Collerson, K.D., Gill, J.B., Deniel, C., 1992. High Th/U ratios in subcontinental lithospheric mantle: mass spectrometric measurement of Th isotopes in Gaussberg lamproites. Earth Planet. Sci. Lett. 111, 257–268.

Wood, B.J., Blundy, J.D., Robinson, J.A.C., 1999. The role of clinopyroxene in generating U-series disequilibrium during mantle melting. Geochim. Cosmochim. Acta 63, 1613–1620.

Wu, Z.C., 1721. Sketch of the Ninggu Tower. The Qing Dynasty Records.

Xu, C.F., 1996. The earthquake distribution and the resistivity structure in the Chinese mainland (1). Acta Seismol. Sin. 18, 254–261.

Zhang, M., Menzies, M.A., Suddaby, P., Thirlwall, M.F., 1991. EM1 signature from the post-Archaean subcontinental lithospheric mantle: isotopic evidence from the potassic volcanic rocks in NE China. Geochem. J. 25, 387–398.

Zhang, M., Suddaby, P., Thompson, R.N., Thirlwall, M.F., Menzies, M.A., 1995. Potassic volcanic rocks in NE China: geochemical constraints on mantle source and magma genesis. J. Petrol. 36, 1275–1303.

Zhang, H.F., Sun, M., Zhou, X.H., Fan, W.M., Zhai, M.G., Yin, J.F., 2002. Mesozoic lithosphere destruction beneath the North China Craton: evidence from major-, trace-element and Sr–Nd–Pb isotope studies of Fangcheng basalts. Contrib. Mineral. Petrol. 144, 241–253.

Zhi, X.C., Song, Y., Frey, F.A., Feng, J.L., Zhai, M.Z., 1990. Geochemistry of Hannuoba basalts, eastern China: constraints on the origin of continental alkalic and theoleiitic basalt. Chem. Geol. 88, 1–33.

Zhou, X.H., Zhu, B.Q., 1992. Study on the isotopic system and mantle chemical zonation of Cenozoic basalts in Eastern China. In: Liu, R. (Ed.), The Age and Geochemistry of Cenozoic Volcanic Rocks in China. Seismology Publishing House, Beijing, pp. 366–391.

Zindler, A., Hart, S.R., 1986. Chemical geodynamics. Annu. Rev. Earth Planet. Sci. 14, 493–571.

Zou, H., Zindler, A., 1996. Constraints on the degree of dynamic partial melting and source composition using concentration ratios in magmas. Geochim. Cosmochim. Acta 60 (4), 711–717.

Zou, H., Zindler, A., 2000. Theoretical studies of ^{238}U–^{230}Th–^{226}Ra and ^{231}Pa–^{235}U disequilibria in young lavas produced during mantle melting. Geochim. Cosmochim. Acta 64 (10), 1809–1817.

Zou, H., Zindler, A., Xu, X., Qi, Q., 2000. Major and trace element, and Nd–Sr–Pb isotope studies of Cenozoic basalts in SE China: mantle sources, regional variations, and tectonic significance. Chem. Geol. 171, 33–47.

Zou, H., Zindler, A., Niu, Y., 2002. Constraints on melt movement beneath the East Pacific Rise from ^{230}Th–^{238}U disequilibrium. Science 295, 107–111.